Green Chemistry

Cutting-edge research for a greener sustainable future

Accepted Manuscript

This article can be cited before page numbers have been issued, to do this please use: Z. Li, J. Zhang, C. Li, J. Cao and S. Tao, *Green Chem.*, 2026, DOI: 10.1039/D5GC06463E.

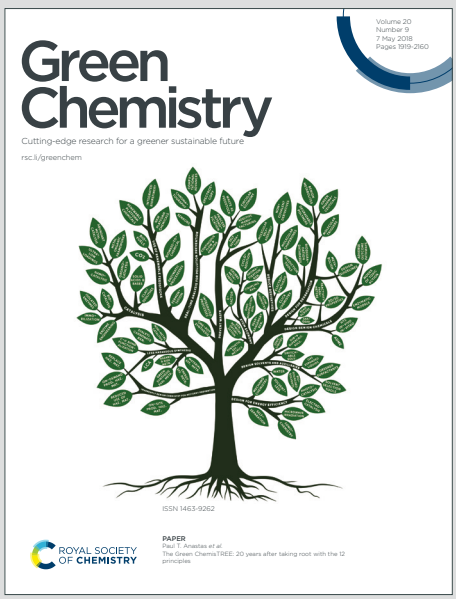

ROYAL SOCIETY OF CHEMISTRY

rsc.li/greenchem

View Article Online
DOI: 10.1039/D5GC06463E

The Green Foundation box

1. This work advances green chemistry by utilizing natural flavonoids extracted from waste orange peel as photocatalysts, replacing traditional toxic, expensive, and multi-step synthetic photosensitizers. The system also enables efficient photocatalytic oxidation reactions in aqueous solvent, reducing the need for organic solvents, achieving a comprehensive green chemistry approach spanning catalyst, solvent, and light source.

2. The specific green chemistry achievements of this work include: using orange peel extract to achieve photocatalytic oxidation of styrene (53.7% conversion) and cyclohexene (up to 86.0% conversion), and efficient oxidation of benzyl alcohol in water (52.4% conversion, >99% selectivity). The entire process avoids metal catalysts and toxic reagents, enabling waste valorization and a green reaction process.

3. This work could be made greener by conducting life cycle assessment (LCA) to quantify its environmental benefits and by investigating catalyst recycling and reusability to further enhance sustainability. Future research could also explore extending the system to other types of biomass waste and attempt to utilize solar energy to drive the reactions, thereby reducing energy consumption and further improving the green credentials of the entire process.

View Article Online
DOI: 10.1039/D5GC06463E

ARTICLE

The AIE-Active Flavonoids in Orange Peel for Photocatalytic Oxidation Reactions

Received 00th January 20xx,
Accepted 00th January 20xx

DOI: 10.1039/x0xx00000x

Zhuxin Li,[a] Junfei Zhang, [a] Chong Li, [b] Jinzhe Cao, *[a] and Shengyang Tao,*[a]

Photochemical organic synthesis has emerged as a prominent and important synthetic methodology in recent years. However, conventional photosensitizers are often expensive and require multi-step synthesis for their preparation. This study utilizes natural flavonoids extracted from citrus peel (Tangeretin, Nobiletin, and Sinensetin) as photocatalysts to achieve the photooxidation of alkenes. Conversion rates of 53.7% for styrene and 66.1% for cyclohexene were attained. Reaction Mechanism Generator (RMG) simulations revealed that alkenes undergo reaction pathways mediated by singlet oxygen or oxygen-free radicals to form the corresponding products, a finding corroborated by a series of control experiments and EPR. These flavonoid compounds exhibit Aggregation-Induced Emission (AIE) characteristics. Upon encapsulation with saponins to form nanoparticles, the conversion rate for cyclohexene was further enhanced to 86.0%. Furthermore, this system successfully achieved the efficient oxidation of benzyl alcohol in an aqueous solvent (52.4% conversion, >99% selectivity). This work establishes a comprehensive green chemistry system encompassing the light source, catalyst, and solvent. The proposed strategy offers a novel approach to the development of natural photocatalysts and sustainable organic synthesis.

1 Introduction

In recent years, photocatalytic strategies have been expanded into the field of organic synthesis for the production of high-value-added chemicals[1,2,3]. Studies have indicated that reactive oxygen species (ROS) such as singlet oxygen ($_1O^2$) and superoxide anion radicals ($\cdot O_2^-$) participate in photocatalytic reactions, contributing to oxidative activity[4]. Typically, oxidants such as H_2O_2 and TBHP (tert-butyl hydroperoxide) are employed to generate these reactive oxygen species, thereby enhancing the reaction's oxidative capacity[5,6]. To substitute these less readily available oxidants with molecular oxygen (O_2) for oxidation reactions, identifying or designing photocatalysts that can efficiently activate O_2 is particularly crucial. Among various photocatalysts, transition metal complexes, such as those based on ruthenium and iridium, have garnered significant attention due to their exceptional photophysical properties, which underpin numerous synthetic reactions. [7,8,9] However, these transition metal complexes suffer from limitations, including low natural abundance, high cost, and considerable toxicity. To overcome these drawbacks, researchers have recently introduced synthetic organic photocatalysts, such as Rhodamine B, Rhodamine 6G, and Eosin Y, for photocatalytic oxidation reactions[10,11,12]. These studies demonstrate that synthetic organic photocatalysts can exhibit catalytic efficiency comparable to, or even superior to, conventional transition metal chromophores. Nevertheless, these organic photocatalysts must be prepared through tedious multi-step syntheses and also possess significant physiological toxicity. Consequently, the search for sustainable, environmentally benign, and readily accessible organic photocatalysts remains a pressing and urgent imperative.

To obtain photocatalysts with the aforementioned properties, we turned our attention to nature. A study by Wang et al. extracted hypericin from St. John's wort flowers and utilized it as an efficient, renewable catalyst in photoredox reactions.[13] Concurrently, molecules exhibiting Aggregation-Induced Emission (AIE) properties have been demonstrated to possess exceptional photosensitizing capabilities, serving as green alternatives for various photocatalytic organic reactions[14]. Naturally occurring flavonoids found in orange peel, such as tangeretin, nobiletin, and sinensetin, possess notable AIE properties, positioning them as a promising class of natural organic photocatalysts. However, to date, these compounds have not been explored within the field of photocatalysis. Given the widespread availability of citrus plants and the excellent photophysical properties of flavonoids, we investigated the potential of these flavonoid compounds as novel and versatile catalysts for photooxidation.

To validate the photocatalytic performance of the flavonoid compounds, we selected the photocatalytic oxidation reactions of styrene and cyclohexene as model transformations[15,16]. The results demonstrated that the flavonoids extracted from orange peel effectively catalyzed these reactions under mild conditions, and the desired products could be isolated without requiring additional purification procedures. To gain further insight into the reaction process

[a] Dalian University of Technology. No.2 Linggong Road, Dalian, Liaoning, China.
[b] Xi′an Modern Chemistry Research Institute, Xi′an 710065, China.
Supplementary Information available: [details of any supplementary information available should be included here]. See DOI: 10.1039/x0xx00000x

and product distribution, we employed a machine learning-based approach for the automated exploration and characterization of chemical reaction networks (CRNs) to investigate the plausible reaction mechanism[17,18]. This methodology enabled the systematic exploration of possible reaction pathways and intermediates, followed by the optimization and simplification of the mechanistic model. Finally, the accuracy of the proposed mechanism was verified through a series of control experiments and EPR.

Leveraging the AIE properties of the flavonoid compounds, we subsequently employed a nanoprecipitation method to form uniform photocatalyst@saponin nanoparticles. This nano-encapsulation strategy further enhanced the conversion rate of cyclohexene. Capitalizing on their AIE behavior, we then applied these nanoparticles in an aqueous system, successfully achieving the efficient oxidation of benzyl alcohol in water as the solvent. These results verify that photocatalysts exhibiting AIE properties exhibit superior photocatalytic performance and can be utilized in environmentally benign aqueous systems, embodying the principle of a holistic green chemistry approach throughout the entire process (Fig. 1).

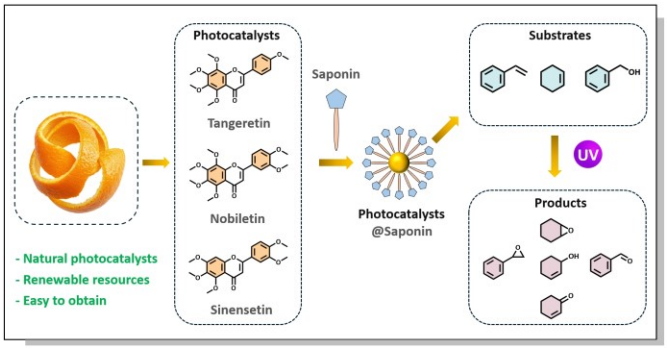

Fig.1 Schematic diagram of flavonoids in orange peel as photooxidation catalysts.

2 Materials and Methods

2.1 Materials and Chemicals

All materials and reagents were obtained from commercial sources and used without any further purification. Fresh citrus fruit was purchased from a local market. The peels were manually separated from the fruits. Standard compounds of tangeretin, nobiletin, and saponins were acquired from Adamas Beta®. The standard of sinensetin was purchased from Aladdin. Solvents used in this study, including methanol, petroleum ether, ethyl acetate, acetonitrile, and glycerol, were all procured from Aladdin. All materials and reagents were of chemical pure (CP) or analytical reagent (AR) grade.

2.2 Extract Analysis

The AIE-active constituents from orange peel were analyzed via extraction and liquid chromatography. Fresh peel was first dried at room temperature for 48 hours. To enhance extraction efficiency and increase the contact surface area between the peel and the extraction solvent, the dried material was ground into a powder using a mortar and pestle and subsequently sieved through a 60-mesh sieve to obtain a homogeneous sample. Twenty grams of this dried powder were then immersed in 20 mL of a solvent mixture consisting of petroleum ether and ethyl acetate (7:3, v/v). The mixture was subjected to ultrasonic extraction at room temperature for 30 minutes. The resulting extract was filtered to obtain the final orange peel extract. The identification of flavonoid compounds within the extract was performed using high-performance liquid chromatography (HPLC) coupled with a diode array detector (DAD). The primary flavonoids previously reported in commercial sources include tangeretin, nobiletin, and sinensetin[19]. Accordingly, these commercial standards were used as references. HPLC analysis of the orange peel extract identified its components by comparing their retention times with those of authentic standards.

All chromatographic analyses for both the extracts and standards were acquired using an Agilent 1260 Infinity II HPLC system equipped with a Sunfire™ C18 column maintained at 25°C. Fluorescence spectra were collected on an Agilent G9800A fluorescence spectrometer. UV-Vis spectra were acquired using a Purkinje General TU-1900 spectrophotometer. Particle size distributions were obtained from an Anton Paar Litesizer™ 500 particle analyzer. The morphology of the AIE nanoparticles was investigated by transmission electron microscopy (TEM) using a JEOL JEM-F200 microscope.

2.3 Electrochemical Property Measurement

All electrochemical measurements were carried out using an electrochemical workstation. A standard three-electrode configuration was employed for all experiments in an acetonitrile-based system: a glassy carbon working electrode, a platinum wire counter electrode, and an $Ag/AgNO_3$ reference electrode. The scan rate was set at 0.2 V/s over a potential range of -2.5 V to +2.5 V. To ensure sufficient conductivity, 0.1 M tetrabutylammonium hexafluorophosphate ($[NBu_4][PF_6]$) in acetonitrile was added as the supporting electrolyte. Under these conditions, cyclic voltammetry (CV) was performed to obtain the voltammograms of the three photocatalysts and all relevant reaction substrates.

2.4 Photocatalytic Experimental Procedure

To evaluate and compare the photocatalytic efficacy, a set of four parallel experiments was designed with the catalyst as the primary variable. The procedure was as follows: Four separate 5 mL vials were prepared. Into three of these vials,5 mg of a single flavonoid standard was added: tangeretin, nobiletin, and sinensetin, respectively. The fourth vial, containing no photocatalyst, served as a blank control. Given the experimental timeline, all three aforementioned photocatalysts were procured from commercial suppliers. Its structure is identical to that of the component extracted from orange peel. Unless otherwise specified, 2 mL of acetonitrile was used as the solvent in each vial, and the substrate (0.1 mmol) was added. Each reaction mixture was purged with a stream of O_2 for 5 minutes to ensure an oxygen-saturated environment. A magnetic stir bar was then added, and the vial

was immediately sealed with a cap containing a PTFE/silicone septum. In the experiment, the distance between the LED and the reaction tube was set at 1 cm, with horizontal irradiation employed. The light source parameters were configured at 365 nm and 6 W. The reaction system was continuously stirred at room temperature and irradiated for 16 hours. This configuration represents an optimal compromise between the high light intensity typical of 5–6 W LEDs and temperature control within the reaction system[20].Upon completion of the reaction, the mixtures were analyzed using Gas Chromatography-Mass Spectrometry (GC-MS) for product identification and quantification. Quantification was performed using the external standard method, with calibrated curves established for the relevant substrates and products.

2.5 Preparation of AIE Nanoparticles

A solution of each photocatalyst (tangeretin, nobiletin, or sinensetin) was prepared in tetrahydrofuran (THF) at a concentration of 5 mg/mL. 1 mL of each photocatalyst solution was separately added dropwise into 0.5 mL of PBS buffer under vigorous stirring. The mixture was stirred continuously at room temperature for 30 minutes to facilitate rapid THF evaporation and the formation of small molecular aggregates. To prepare photocatalyst@saponin nanoparticles, 200 μL of saponin solution (1 mg/mL) was subsequently added to the mixture. The resulting suspension was stirred for 120 minutes at room temperature to ensure complete formation and stabilization of the nanoparticles. The obtained nanoparticles were characterized immediately after preparation and subsequently subjected to evaluation of their photocatalytic performance.

2.6 Reaction Network Prediction Methodology

The exploration of potential reaction mechanisms and pathways was conducted using the Reaction Mechanism Generator (RMG) software, an open-source toolkit for the automated construction of chemical kinetic models. The simulation was performed under the following conditions: The reaction system was specified to occur in the liquid phase at a constant temperature of 298 K, with a total reaction time of 16 hours, ensuring consistency with the actual experimental conditions. Furthermore, the error tolerance for reaction flux and thermodynamic estimates was set to 0.1, a value that falls within the recommended optimal range as specified in the official user guide.

3 Results and Discussion

3.1 Characterization of Orange Peel Extract

Chromatographic analysis revealed the presence of multiple components in the citrus peel extract (Fig.2A). By comparing retention times with authentic standards (Table S1), three major constituents were identified as flavonoids: peak 1 (sinensetin), peak 2 (nobiletin), and peak 3 (tangeretin). For peak 4 observed in the extract, its significantly different retention time suggested a structural dissimilarity to the primary flavonoid compounds, leading to its exclusion from further consideration. This preliminary identification was subsequently validated by liquid chromatography coupled with high-resolution mass spectrometry (LC-HRMS), as shown in Fig.S4-S7. Based on the comparison of peak areas, the extraction yield from 50 g of waste citrus peel was determined to be approximately 1 mg of total flavonoids. This yield provides a foundational basis for potential process scale-up and the development of low-cost experiments.

To verify the AIE characteristics of the three flavonoids, their ultraviolet-visible (UV-Vis) absorption spectra were first recorded in methanol solution. As shown in Fig.2B, the primary absorption peaks of all three flavonoids were observed between 320 nm and 335 nm, which is attributed to intramolecular charge transfer (ICT). In the range of 245 nm to 275 nm, tangeretin exhibited one secondary absorption peak, while both nobiletin and sinensetin displayed two secondary peaks, corresponding to π→π* transitions within the molecules. Subsequently, the fluorescence behavior of these compounds was investigated in mixtures of glycerol and methanol. As depicted in Fig.2C, sinensetin exhibited nearly negligible fluorescence emission in pure methanol. However, a gradual enhancement in fluorescence intensity was observed as the glycerol fraction increased from 0% to 90%. This phenomenon indicates that the viscous medium restricts intramolecular rotation (RIR), effectively suppressing non-radiative decay pathways and thereby leading to a significant enhancement in fluorescence emission. Notably, as shown in Fig.2D, a red shift in the emission wavelength of sinensetin occurred with increasing glycerol fraction. This behavior is likely due to facilitated intermolecular charge transfer in the aggregated or more rigid state. Tangeretin and nobiletin demonstrated similar trends in their photophysical properties, as shown in Fig.S8. In conclusion, the collective experimental results confirm that all three compounds exhibit characteristics typical of AIE-active materials.

The catalytic performance of a photocatalyst in photoredox reactions is primarily determined by its photophysical properties and electrochemical behavior in both the ground and excited states[21]. Therefore, understanding and evaluating these characteristics is essential for predicting how the photocatalyst will interact with reaction components during photocatalytic oxidation experiments. The excited-state energy (E_{00}) represents the energy difference between the ground state and the excited state, indicating the minimum energy required to reach the excited state. A higher E_{00} value generally correlates with stronger photoreduction and photooxidation capabilities. However, this value must be sufficiently low to allow for excitation under ultraviolet or visible light irradiation. The E_{00} value can be determined spectroscopically and calculated using equation (1). Among them, h is the Planck constant, c is the speed of light, and λ_{max} is the maximum wavelength of absorption present in the ultraviolet-visible spectrum.

$$E_{00} = \frac{hc}{\lambda max} \quad (1)$$

View Article Online
DOI: 10.1039/D5GC06463E

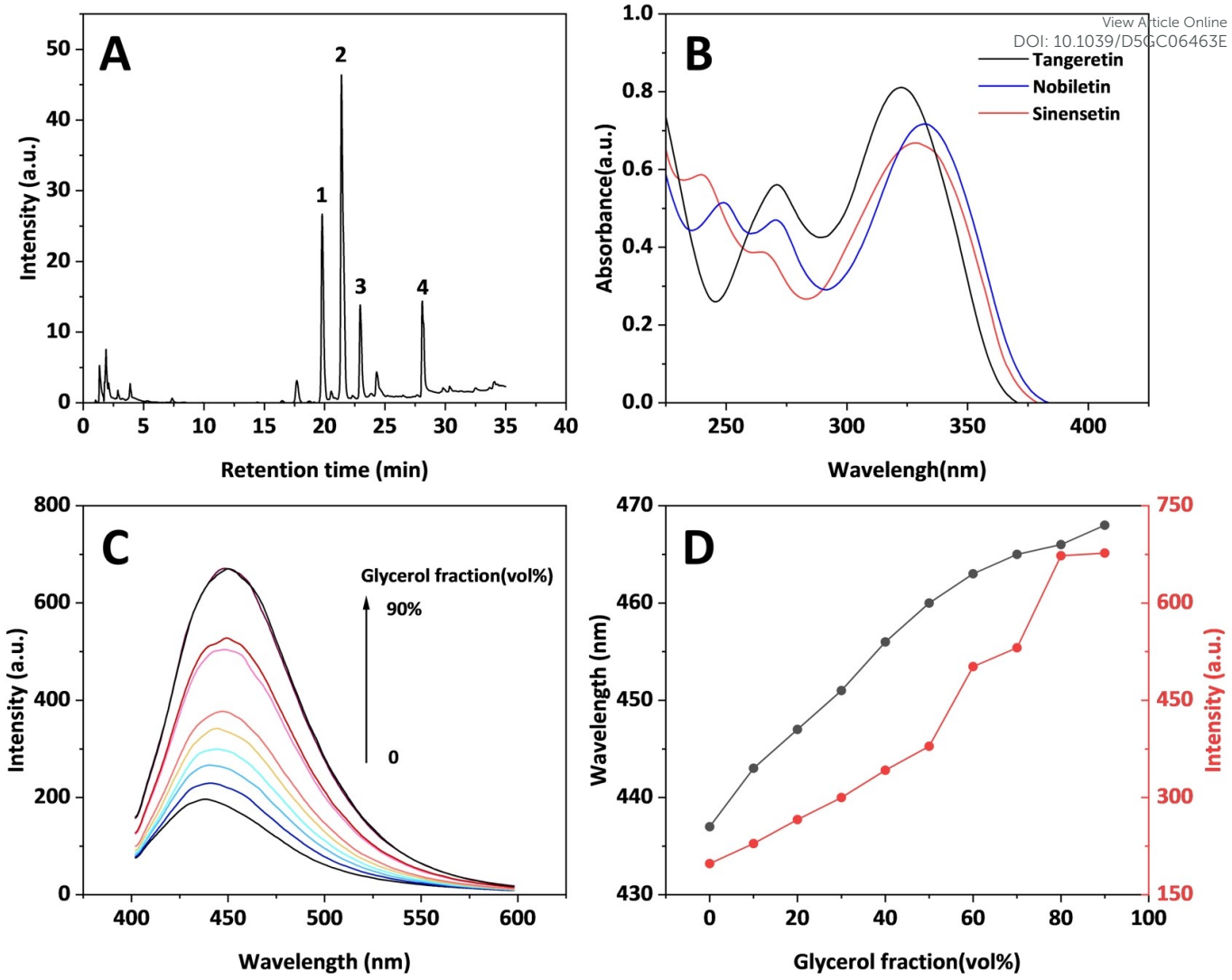

Fig.2 HPLC results of orange peel extract (A). UV-visible spectra of three flavonoids (B). PL spectrum of sinensetin in methanol solution with different concentrations of glycerol (C). Illustration of the red line of the maximum emission intensity and the black (D).

The ground-state redox potentials are typically measured using cyclic voltammetry. The ground-state oxidation potential and reduction potential correspond to the first single-electron oxidation process and the first single-electron reduction process of the photocatalyst, respectively[22]. For irreversible voltammograms, the value of E can be approximated as the potential at the peak maximum (E_p) or the half-peak potential ($E_{p/2}$) .[23]

The photoreduction and photooxidation capabilities of a photocatalyst depend on its excited-state redox potentials, which correspond to the single-electron redox reactions of the photoexcited photocatalyst (*photocatalyst). Typically, the excited-state reduction potential ($^*E_{red}$) and excited-state oxidation potential ($^*E_{ox}$) are not directly measured but are calculated using the excited-state energy and standard ground-state redox potentials, as shown in equations (2) and (3).

$$^*E_{red} = E_{red} + E_{00} \quad (2)$$

$$^*E_{ox} = E_{ox} - E_{00} \quad (3)$$

To this end, we calculated the excited-state energies (E_{00}) of three flavonoids in methanol solution from their UV-visible absorption spectra, as presented in Table 1. All three compounds exhibited high E_{00} values, with tangeretin reaching a value of up to 3.36 eV. Subsequently, the ground-state oxidation and reduction potentials of these flavonoids and all relevant reaction substrates were measured using cyclic voltammetry (Fig.S9). Finally, the excited-state redox potentials were calculated using equations (2) and (3) to evaluate their photo-redox properties, with the results summarized in Table 1 and Table S2. All three flavonoids demonstrated significant potential as photocatalysts. Their excited-state reduction potentials exceeded 2.0 V (vs. $Ag/AgNO_3$), indicating strong oxidizing capabilities upon photoexcitation, which can facilitate the generation of highly oxidative species. The half-wave oxidation potentials of all reaction substrates were below 1.9 V, which is also lower than the reduction potentials of the excited states of the three aforementioned flavonoid compounds. This result theoretically confirms the thermodynamic feasibility of the proposed reaction[24].

View Article Online
DOI: 10.1039/D5GC06463F

Table 1 Photophysical constants of three photocatalysts.

	Tangeretin	Nobiletin	Sinensetin
E_{00}/eV	3.36	3.31	3.27
E_{red}/V	-0.95	-1.20	-1.26
E_{ox}/V	+1.04	+0.97	+0.98
*E_{red}/V	+2.41	+2.11	+2.01
*E_{ox}/V	-2.32	-2.34	-2.29

3.2 Evaluation of Photocatalytic Performance

To evaluate the photocatalytic performance of the aforementioned three flavonoids, we applied them to the photocatalytic oxidation of styrene. The conversion of styrene to styrene oxide holds significant industrial relevance, primarily yielding two products: styrene oxide (1) and benzaldehyde (2). Styrene oxide is primarily used as an intermediate in the production of pharmaceuticals and fragrances, while benzaldehyde serves as a key chemical feedstock for these applications. The experimental results are summarized in Table 2. In the absence of a photocatalyst, the conversion of styrene was low (19.4%), with a product selectivity ratio of approximately 1:1 for compounds 1 and 2. Upon the addition of a photocatalyst, the conversion of styrene increased significantly: by 10.2% with tangeretin, 34.3% with nobiletin, and 11.7% with sinensetin. These results demonstrate that all three flavonoid photocatalysts exhibited pronounced photocatalytic activity, with nobiletin showing the most outstanding performance. Variations in product selectivity were observed depending on the photocatalyst used. With tangeretin and sinensetin, over 90% of the products favored benzaldehyde. In contrast, under nobiletin catalysis, the product selectivity was lower, with approximately 20% styrene oxide and 80% benzaldehyde being formed.

Table 2 Styrene photocatalytic oxidation results.

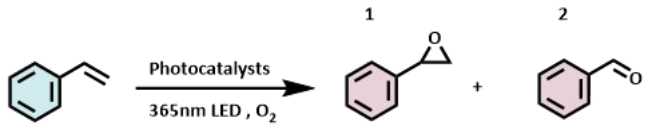

Entry	Photocatalysts	Conv. (%)	Yield 1(%)	Yield 2(%)
1	None	19.4	7.4	12.0
2	Tangeretin	29.6	1.2	28.4
3	Nobiletin	53.7	12.6	41.1
4	Sinensetin	31.1	3.0	28.1

To demonstrate the generality of the three photocatalysts, we further conducted the photocatalytic oxidation of cyclohexene under identical reaction conditions. Cyclohexene is an industrially inexpensive, abundant, and readily available feedstock. Despite its simple chemical structure, its oxidation yields a mixture of products with varying oxidation states and functional groups, as shown in Table 3. To further validate the photocatalytic performance of the three flavonoids, we monitored the time-dependent progress of the photochemical reaction, with the results presented in Fig. 3. In the absence of a photocatalyst, the conversion of cyclohexene was low, reaching only 25.2% after 16 hours of reaction. In contrast, upon the addition of any of the three catalysts, the substrate conversion significantly increased, exceeding 50% in all cases. Notably, when nobiletin was used as the photosensitizer, the highest conversion (66.1%) was achieved. This further corroborates the excellent photocatalytic performance of the three flavonoids in photocatalytic reactions. In the product distribution, cyclohexenol consistently emerged as the major product. In the nobiletin-catalyzed system, the yield of cyclohexenone was comparable to that of cyclohexenol, whereas this phenomenon was not observed in the other systems. It suggests that nobiletin may alter product selectivity, exhibiting distinct catalytic properties compared to the other catalysts.

Table 3 Cyclohexene photocatalytic oxidation results.

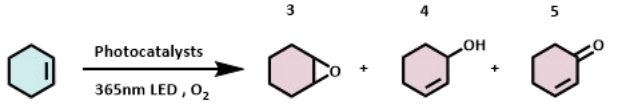

Entry	Photocatalysts	Time (h)	Conv. (%)	Yield3 (%)	Yield4 (%)	Yield5 (%)
1	None	4	3.0	0	1.2	1.8
2	None	8	12.2	1.2	6.4	4.6
3	None	16	25.2	3.3	13.9	8.0
4	Tangeretin	4	20.5	4.3	7.5	8.7
5	Tangeretin	8	30.3	6.8	11.7	11.8
6	Tangeretin	16	54.8	13.5	27.1	14.2
7	Nobiletin	4	33.5	3.7	13.6	16.2
8	Nobiletin	8	55.1	8.0	24.3	22.8
9	Nobiletin	16	66.1	8.6	28.9	28.6
10	Sinensetin	4	22.5	4.3	9.7	8.5
11	Sinensetin	8	42.9	8.6	21.4	12.9
12	Sinensetin	16	53.5	11.2	26.7	15.6

3.3 Reaction Network Analysis

Based on the experimental results, we further investigated the reaction mechanism for the nobiletin-catalyzed photooxidation of cyclohexene. To gain a deeper insight into the initiation process and reaction pathways, simulations were performed using the Reaction Mechanism Generator (RMG), an open-source tool developed by the Massachusetts Institute of Technology. [25-28] RMG automates the construction of kinetic models by integrating reaction template libraries, thermodynamic databases, and rate rule estimations to systematically explore plausible reaction pathways and intermediates, subsequently optimizing and simplifying the proposed mechanism. The initial simulation generated a model comprising 1745 species and 6545 reactions. To enhance computational tractability and focus on chemically relevant species, multi-cyclic compounds and biradicals were filtered out. This refinement resulted in a reduced network containing 24 core species and 35 core reactions, which was used to construct the final chemical reaction network. Two primary pathways were identified for the photooxidation of cyclohexene using molecular oxygen: a non-radical pathway and a radical pathway[29]. The non-radical route proceeds via a singlet oxygen-mediated type II photosensitization process, [30] while the radical

View Article Online
DOI: 10.1039/D5GC06463E

ARTICLE

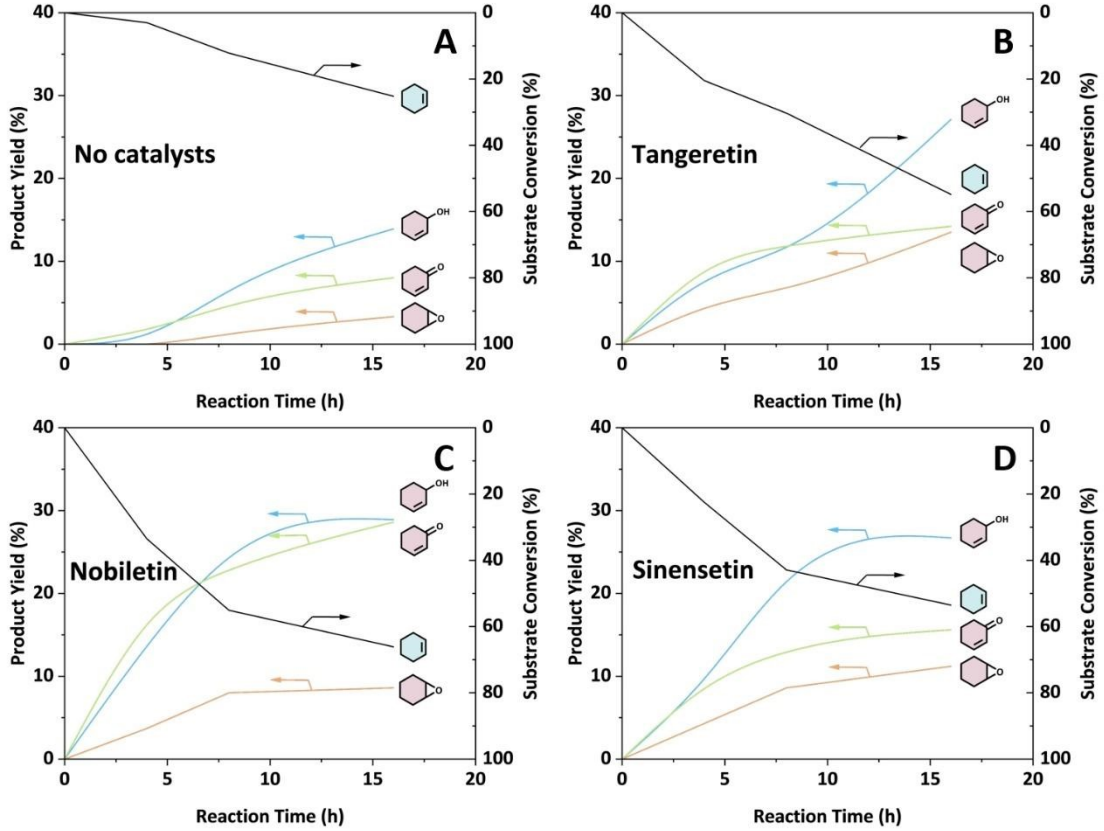

Fig.3 The changes in conversion rate and yield over time without a catalyst (A). Under the presence of a catalyst, the changes in conversion rate and yield over time are observed (B, C, D).

pathway involves an oxygen radical-mediated type I photosensitization mechanism. [31] Based on this analysis, we propose a dual-pathway reaction mechanism for the nobiletin-catalyzed oxidation of cyclohexene, wherein both type I and type II photosensitization reactions operate concurrently (Fig.4).

As illustrated in Fig.4A, under 365 nm light irradiation, nobiletin is photoexcited to its excited state, which subsequently transfers energy to ground-state molecular oxygen, generating highly reactive singlet oxygen while nobiletin returns to its ground state. Singlet oxygen, the primary reactive oxygen species (ROS) in type II mechanisms, acts as an electrophile and initiates the type II photosensitization pathway via a characteristic Schenck ene reaction with cyclohexene. It leads to the formation of an unstable peroxirane intermediate, which undergoes various bond cleavage and rearrangement processes to yield allylic hydroperoxides of cyclohexene. These hydroperoxides subsequently undergo allylic rearrangement or react with additional cyclohexene substrate to form cyclohexenone and water or epoxycyclohexane and cyclohexenol, respectively. We further propose that the reaction does not proceed exclusively via the ene addition

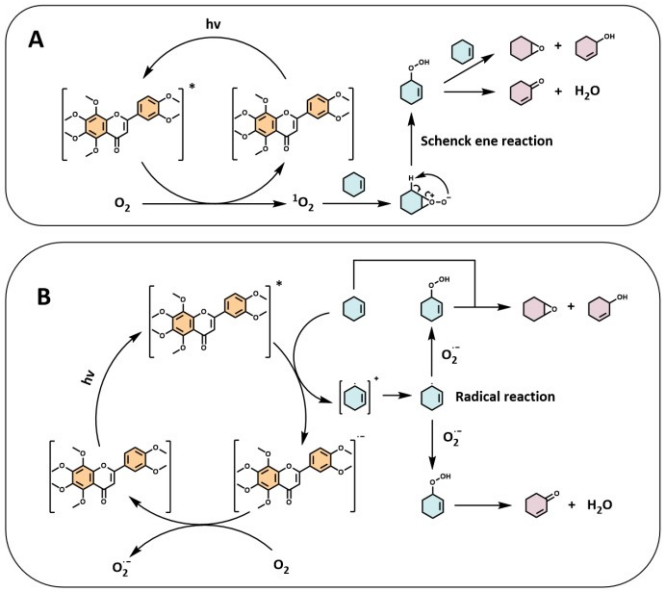

Fig.4 Type II photosensitization reaction mechanism (A). Type I photosensitization reaction mechanism (B).

View Article Online
DOI: 10.1039/D5GC06467F

pathway but is accompanied by a parallel type I photosensitization process (Fig.4B). This pathway generates oxygen-centered radicals that mediate free radical chain reactions, ultimately contributing to the formation of the observed oxidation products.

To further elucidate the photocatalytic oxidation mechanism, a series of control experiments was conducted, as summarized in Fig.5. Initially, the reaction was performed in the absence of light (Condition A). Negligible product formation was observed, confirming that light irradiation is essential for the reaction to proceed. When molecular oxygen was replaced with N_2 (Condition B), the reaction was largely suppressed, indicating that O_2 is indispensable for the oxidation process. Furthermore, upon addition of 3 equivalents of 1,4-benzoquinone (a known superoxide radical anion scavenger, Condition C), the overall reaction extent was reduced. Specifically, the yield of epoxycyclohexane decreased by approximately 60%, while the yields of both cyclohexenol and cyclohexenone increased by about 20%. These results suggest that superoxide radical anions are involved in the process. More importantly, they indicate that the Type I photosensitization pathway predominantly contributes to the formation of epoxycyclohexane. When this pathway is inhibited, the Type II photosensitization route becomes more dominant, resulting in an increased formation of cyclohexenol and cyclohexenone. When 3 equivalents of furfuryl alcohol (a potent singlet oxygen scavenger that can also quench oxygen-centered radicals to some extent) were introduced into the reaction mixture (Condition D), the reaction was quenched entirely. Since furfuryl alcohol effectively inhibits both Type I and Type II pathways, this result provides strong evidence that singlet oxygen is also actively involved in the catalytic cycle. Electron paramagnetic resonance (EPR) experiments were conducted using TEMP and DMPO as spin-trapping agents to further characterize the reactive oxygen species (ROS) in Fig.5E, F. No generation of singlet oxygen or superoxide radicals was detected under dark conditions. However, after 5 minutes of irradiation with 365 nm light, distinct signals corresponding to both ROS were observed. As shown in Fig.5E, three characteristic signals corresponding to singlet oxygen were observed in the range of 3340–3420 G. Their intensity increased with prolonged irradiation time, demonstrating a corresponding rise in the yield of singlet oxygen under illumination. Similarly, Fig.5F displays four characteristic peaks of superoxide radicals within the same magnetic field range, whose intensity also grew with extended light exposure[32,33]. Furthermore, symmetric signals for singlet oxygen and superoxide radicals were observed at g-factors of 2.0060 and 2.0059, respectively. These values show excellent agreement with those reported in the literature[34]. Based on this evidence, the presence of both reactive oxygen species was successfully confirmed. The EPR analysis revealed that the relative intensity of superoxide radicals was weaker than that of singlet oxygen, indicating the predominance of a singlet oxygen-mediated pathway. This observation further validates the accuracy of our proposed mechanism. Based on the collective evidence from these controlled experiments and EPR, the proposed dual-pathway reaction mechanism is successfully validated.

3.4 Photocatalytic Applications of AIE Nanoparticles

Although the three aforementioned photocatalysts demonstrated promising potential in the photooxidation of

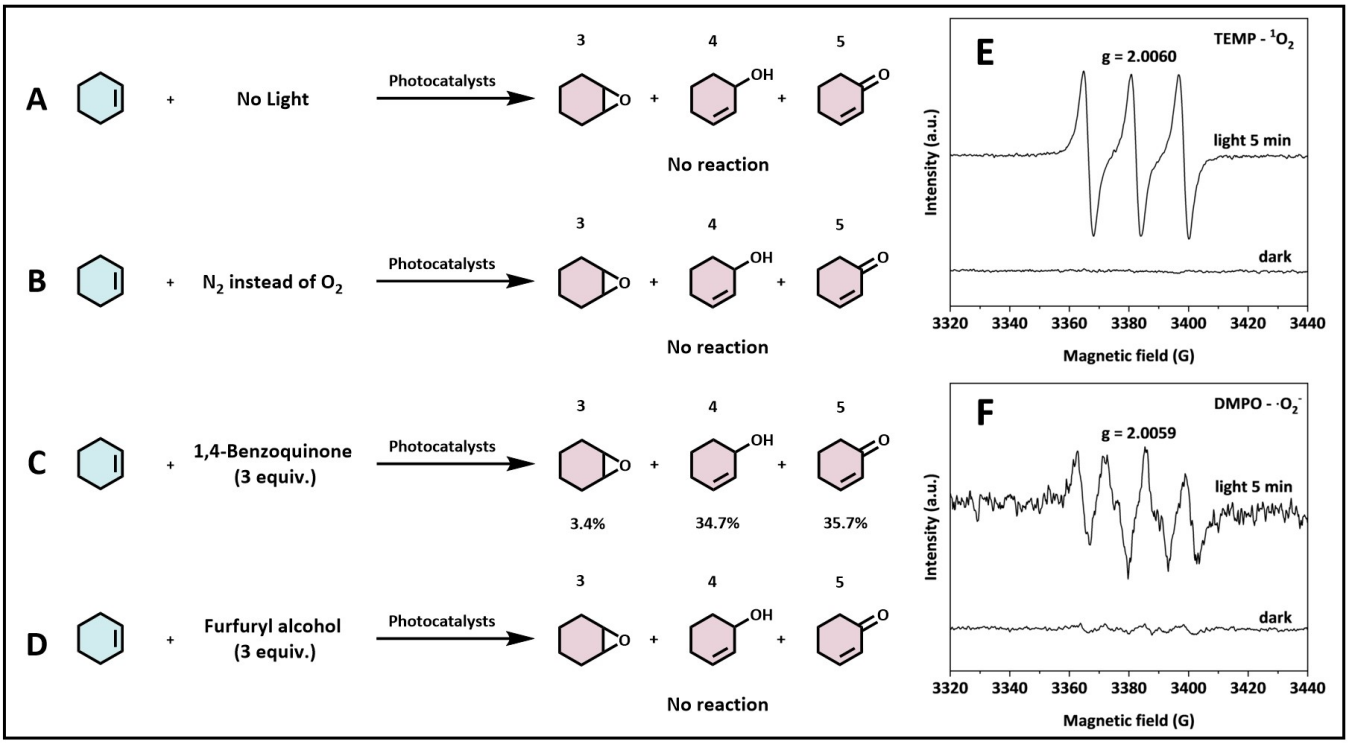

Fig.5 Control Experiments(A,B,C,D). EPR experiments(E,F).

cyclohexene, their intrinsic AIE properties remained underutilized. In the acetonitrile reaction system, these molecules dissolved well, which limited their luminescence and light absorption efficiency due to the lack of aggregation. We reasoned that leveraging their AIE characteristics by inducing aggregation in an aqueous solution could significantly enhance their luminescence and light absorption, thereby substantially improving their photocatalytic performance[35]. A straightforward method for preparing AIE-active micelles involves encapsulating AIEgens within amphiphilic, non-luminescent micellar structures to induce aggregation and obtain luminescent nanoparticles. Saponins, a class of amphiphilic steroidal and triterpenoid glycosides widely found in various plants[36], exhibit excellent encapsulation capabilities in aqueous solutions due to their inherent hydrophobicity[37]. Therefore, we employed a nanoprecipitation method to form uniform photocatalyst@saponin nanoparticles, as detailed in Section 2.6. The size and polydispersity of the resulting photocatalyst@saponin nanoparticles were analyzed using dynamic light scattering (DLS), and their morphology was examined by transmission electron microscopy (TEM). The results are presented in Fig. S10 of the Supporting Information. The pure saponin nanoparticles exhibited a hydrodynamic diameter of 690 nm with a polydispersity index (PDI) of 0.226. Upon encapsulation of the three flavonoid AIE molecules, the hydrodynamic diameters of all photocatalyst@saponin nanoparticles increased significantly, by 120-260 nm, compared to the pure saponin nanoparticles. The PDI of the particles also increased to some extent. This size enlargement indicates the formation of aggregates and suggests the successful coating of an additional layer around the AIE nanoparticles, forming a core-shell structure. TEM images revealed that the particles maintained a spherical morphology before and after encapsulation, with no noticeable change in their overall shape.

To verify the photocatalytic activity of the flavonoid photocatalyst@saponin nanoparticle system, we conducted photocatalytic oxidation experiments of cyclohexene under conditions where the amount of flavonoid photocatalyst remained constant while only its aggregation state was varied. The results are summarized in Table 4. According to the control group data, the substrate conversion rate was 25.2% before the addition of saponin particles and 22.0% after, indicating that the influence of pure saponin particles on the reaction is negligible. A comparison of the data from groups 2, 3, and 4 reveals that encapsulating the photocatalyst with saponin to induce aggregation enhanced the substrate conversion rate by 10–20%, with the nobiletin group exhibiting the most significant improvement, achieving a 19.9% increase in conversion. These results demonstrate that the photocatalytic performance was further enhanced after aggregation of the photocatalyst and the manifestation of aggregation-induced emission (AIE) characteristics. This improvement may be attributed to the enhanced utilization of light energy following molecular aggregation, thereby increasing the photocatalytic efficiency. Additional theoretical evidence is provided in Fig. S11, where we measured the fluorescence spectra of Nobiletin nanoparticles, free Nobiletin, and pure saponin particles. The spectra clearly show that the pure saponin particles are virtually non-emissive. More importantly, the Nobiletin nanoparticles in their aggregated state exhibited a higher relative fluorescence intensity and a red-shifted emission maximum compared to the free Nobiletin molecules. This provides direct photophysical proof of effective AIE, theoretically supporting the claim that the AIE property directly contributes to the enhanced photocatalytic performance. Meanwhile, the modified photocatalyst exhibits photocatalytic performance on a par with traditional metal-based photocatalysts or organic dyes[38-40] (Table S3). Based on the catalyst cycling experiments conducted over four cycles, the sustainability of the three aforementioned photocatalysts was evaluated. As illustrated in Fig. S12, all three flavonoid-based photocatalysts experienced a decline in content after the first cycle, with residual amounts remaining around 80%. With successive cycles, a continued decrease in content was observed, which may be attributed to the inherent biodegradability of these natural flavonoid compounds.

Table 4 Nanoparticle-catalyzed cyclohexene results.

Entry	Photocatalysts	Time (h)	Conv. (%)	Yield3 (%)	Yield4 (%)	Yield5 (%)
1	None	16	22.0	3.4	12.7	5.9
2	Tangeretin	16	62.9	15.8	29.8	17.3
3	Nobiletin	16	86.0	11.2	37.6	37.2
4	Sinensetin	16	65.5	14.7	32.1	18.7

Given that the saponin-coated AIE nanoparticles exhibit excellent dispersibility in water, we further constructed an aqueous-phase photocatalytic system, aiming to achieve a fully green chemical process from photocatalyst to solvent. Benzyl alcohol, as a classic fine chemical raw material, is widely utilized in the pharmaceutical, fragrance, and agrochemical industries. Therefore, we applied the aforementioned photocatalyst nanoparticles to the photocatalytic oxidation of benzyl alcohol, with the results presented in Table 5. Pure saponin nanoparticles exhibited almost no catalytic activity toward the oxidation of benzyl alcohol, with negligible conversion observed after 16 hours of illumination. In contrast, upon the addition of the photocatalyst, the conversion rates reached 43.5%, 52.4%, and 42.5%, respectively, demonstrating that the photocatalyst nanoparticles also perform effectively in aqueous systems, with selectivity consistently reaching 99%. However, when unmodified pure photocatalysts (such as Nobiletin) were directly dispersed in water for the photo-oxidation reaction, the substrate conversion reached only about 55% of that achieved by the Nobiletin nanoparticle system. This result confirms that the saponin-encapsulated photocatalyst more effectively exhibits AIE properties, thereby significantly enhancing photocatalytic performance in aqueous systems. These results indicate that a fully green photochemical oxidation reaction can be achieved in water using entirely natural compounds.

View Article Online
DOI: 10.1039/D5GC06165F

Table 5 Oxidation results of benzyl alcohol.

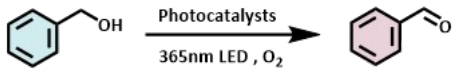

Entry	Photocatalysts	Solvent	Time (h)	Conv. (%)	Select. (%)
1	None	H_2O	16	0	0
2	Tangeretin[a]	H_2O	16	43.5	>99
3	Nobiletin[a]	H_2O	16	52.4	>99
4	Sinensetin[a]	H_2O	16	42.5	>99
5	Nobiletin[b]	H_2O	16	29.1	>99

[a]Saponin-based nanoparticle system. [b]Simply dispersed in water.

3.5 Green Metrics

One of the simplest metrics for evaluating the environmental friendliness of a process—particularly with respect to waste generation—is the Environmental Factor (E-factor)[41]. The E-factor quantifies the waste generated by a process, expressed as kilograms of waste per kilogram of product, as shown in equations (4).

$$\text{E-factor} = \frac{\text{mass of wastes}}{\text{mass of products}} \quad (4)$$

Waste includes all materials other than the target product, and the ideal E-factor is 0. In contrast, a higher E-factor indicates greater waste generation and consequently a larger negative environmental impact. Typically, the majority of emitted waste consists of the large volumes of solvents used in chemical reactions, many of which are non-renewable and toxic, with the potential to cause environmental harm. According to published guidelines for green solvent selection, water is recognized as the greenest solvent, while acetonitrile is also among the recommended options[42]. This aligns with the green solvents employed in our experiments, reflecting our commitment to a holistic green chemistry approach encompassing both the photocatalyst and the solvent system. In addition, Atom Economy (AE) is widely recognized as a simple, practical, and effective green metric for chemical reactions[43]. Based on the aforementioned methodology of green chemistry metrics, we calculated the relevant indicators for the photocatalytic oxidation of benzyl alcohol. The results are summarized in Table S4. The results indicate that all three catalytic reactions exhibit excellent atom economy (AE = 85% for all). Furthermore, the use of water as the solvent resulted in a zero solvent-related environmental impact, significantly reducing the overall process environmental footprint. In addition, all three photocatalysts achieved E-factors below 2.5, a value substantially lower than those typical of conventional organic synthesis or pharmaceutical processes[44], demonstrating the successful implementation of a fully green chemistry approach.

4 Conclusion

This study represents the first introduction of natural flavonoid compounds with aggregation-induced emission (AIE) characteristics into the field of photocatalysis. Utilizing flavonoids extracted from citrus resources as novel and sustainable photocatalysts, efficient photocatalytic oxidation of styrene and cyclohexene was achieved, demonstrating excellent atom economy and operational simplicity. Reaction mechanism simulations (RMG), control experiments and EPR revealed a dual-pathway react ion mechanism mediated by photogenerated singlet oxygen and oxygen radicals, providing a theoretical foundation for the rational design of natural product-based photocatalysts. Furthermore, luminous nanoparticles with high light absorption efficiency were constructed using natural saponin micelle encapsulation technology and successfully applied in an environmentally friendly aqueous catalytic system, resulting in significantly enhanced conversion of cyclohexene and efficient oxidation of benzyl alcohol in water. This work, utilizing waste orange peel as a raw material, expands the application boundaries of biomass resources in photocatalytic organic synthesis. It shows potential for extension to aqueous-phase C–H bond activation and other fields, offering new insights for the development of efficient, sustainable, and low-cost green catalytic systems.

Author contributions

ZL: Conceptualization, writing – original draft, writing – review & editing. JZ: Writing – review & editing. CL: Writing – review & editing. JC: Writing – review & editing. ST: Conceptualization, Funding acquisition, writing – review & editing.

Conflicts of interest

There are no conflicts to declare.

Data availability

All data supporting the findings of this study are available within the paper and its SI: the relevant experimental operations described in the text and other results.

Acknowledgements

The authors would like to acknowledge the financial support from the National Natural Science Foundation of China (No. 22372025, 22272017, 22402158), and the Fundamental Research Funds for the Central Universities (No.DUT25Z2722, DUT22LAB607).

References

1 K. Li, R. K. Xie, Z. Y. Wang, *Chem. Eng. J.*, 2025, **516**, 163950.
2 W. Zhang, Z. Lu, C. Chen, *Small*, 2025, **21**, 2502316.
3 T. X. Luan, L. B. Xing, N. Lu, *J. Am. Chem. Soc.*, 2025, **147**, 12704 – 12714.
4 N. Wen, Y. P. Huang, Y. T. Yang, *ACS Catal.*, 2024, **14**, 11153 – 11163.
5 J. Tang, Z. Jiang, Z. Gao, *Angew. Chem. Int. Ed.*, 2025, **64**, e202416879.
6 P. K. Bagad, R. S. Darole, G. R. Krishna, *J. Org. Chem.*, 2024, **89**, 9371 – 9380.
7 H. T. Gong, L. Zhang, C. H. Deng, *J. Am. Chem. Soc.*, 2025, **147**, 9134 – 9146.
8 J. Pöhlmann, B. B. Yuan, R. Purushothaman, *ACS Catal.*, 2025, **15**, 10542 – 10549.

View Article Online
DOI: 10.1039/D5GC06463E

9 E. Bednářová, R. Grotjahn, C. X. Lin, *J. Am. Chem. Soc.*, 2025, **147**, 12511 – 12522.
10 Y. Y. Zhao, D. Wang, G. T. Sun, *Chem. Eng. J.*, 2025, **518**, 164759.
11 H. I. Coskun, F. De Luca Bossa, X. L. Hu, *J. Am. Chem. Soc.*, 2024, **146**, 28994 – 29005.
12 J. Y. Rui, X. P. Mu, J. Soller, *Nat. Catal.*, 2024, **7**, 1394 – 1403.
13 J. J. Wang, K. Schwedtmann, K. Liu, *Green Chem.*, 2021, **23**, 881 – 888.
14 R. Hojo, A. M. Polgar, Z. M. Hudson, *ACS Sustain. Chem. Eng.*, 2022, **10**, 9665 – 9678.
15 J. Wang, S. Qiao, M. Yang, *Small*, 2025, **2**, 2409292.
16 J. Büker, X. B. Huang, J. Bitzer, *ACS Catal.*, 2021, **11**, 7863 – 7875.
17 J. P. Unsleber, M. Reiher, *Annu. Rev. Phys. Chem.*, 2020, **71**, 121 – 142.
18 M. Meuwly, *Chem. Rev.*, 2021, **121**, 10218 – 10239.
19 C. Guo, Y. X. Shan, Z. Q. Yang, *J. Sci. Food Agric.*, 2020, **100**, 2664 – 2674.
20 S. A. E. A. Rizvi, Y. Zhou, K. Gong, *Green Chem*., 2023, **25**, 169-172.
21 Y. Y. Wu, D. Y. Kim, T. S. Teets, *Synlett*, 2022, **33**, 1154 – 1179.
22 N. Elgrishi, K. J. Rountree, B. D. McCarthy, *J. Chem. Educ.*, 2018, **95**, 197 – 206.
23 L. Buzzetti, G. E. M. Crisenza, P. Melchiorre, *Angew. Chem. Int. Ed.*, 2019, **58**, 3730.
24 Z. Zhu, X. Wu, Z. Li, *Acc. Chem. Res.*, 2025, **58**, 1094-1108.
25 C. W. Gao, J. W. Allen, W. H. Green, *Comput. Phys. Commun.*, 2016, **203**, 212 – 225.
26 M. J. Liu, A. Grinberg Dana, M. S. Johnson, *J. Chem. Inf. Model.*, 2021, **61**, 2686 – 2696.
27 M. S. Johnson, X. R. Dong, A. Grinberg Dana, *J. Chem. Inf. Model.*, 2022, **62**, 4906 – 4915.
28 A. Grinberg Dana, M. S. Johnson, J. W. Allen, *Int. J. Chem. Kinet.*, 2023, **55**, 300 – 323.
29 I. M. Denekamp, M. Antens, T. K. Slot, *ChemCatChem*, 2018, **10**, 1035.
30 J. Y. Zhang, S. H. Wu, X. M. Lu, *ACS Nano*, 2019, **13**, 14152-14161.
31 K. X. Teng, N. Niu, *Nat. Commun.*, 2022, **13**, 6179.
32 J. Liu, Y. Dong, L. Zhang, *J. Cleaner Prod.*, 2021, **322**, 129059.
33 S. K. Kuk, S. M. Ji, S. Kang, *Appl. Catal., B*, 2023, **328**, 122463.
34 Z. Barbieriková, M. Mihalíková, V. Brezová, *Photochem. Photobiol.*, 2012, **88**, 1442-1454.
35 C. Q. Ma, N. Han, Y. Wang, *Dyes Pigments*, 2023, **211**, 111076.
36 I. Barr, A. Sjölander, J. Cox, *Adv. Drug Delivery Rev.*, 1998, **32**, 247.
37 A. Nicol, R. T. K. Kwok, C. P. Chen, *J. Am. Chem. Soc.*, 2017, **139**, 14792-14799.
38 H. Noh, Y. Cui, A. W. Peters, *J. Am. Chem. Soc.*, 2016, **138**, 14720-14726.
39 H. Yu, X. Wang and T. Kong, *Chem. Commun.*, 2024, **60**, 15051-15054.
40 V. P. Chauke, Y. Arslanoglu, T. Nyokong, *J. Photochem. Photobiol., A*, 2011, **221**, 38-46.
41 C. T. Matos, L. Gouveia, A. R. C. Morais,*Green Chem.*, 2013,**15**, 2854-2864.
42 F. P. Byrne, S. Jin, G. Paggiola, *Sustain. Chem. Process.*, 2016, **4**, 7.
43 B. Trost, *Science*, 1991, **254** , 1471-1477.
44 M. Tobiszewski, M. Marć, A. Gałuszka, *Molecules*, 2015, **20**, 10928-10946.

View Article Online
DOI: 10.1039/D5GC06463E

Data availability

All data supporting the findings of this study are available within the paper and its SI: the relevant experimental operations described in the text and other results.